Revealing the effect of interstitial oxygen on the low-energy crystal electric field excitations of Pr3+ in 214-nickelates

Rajesh Dutta, Avishek Maity, Anna Marsicano, J. Ross Stewart, Matthias Opel, and Werner Paulus

Revealing the effect of interstitial oxygen on the low-energy crystal electric field excitations of Pr^{3+} in *214*-nickelates

Rajesh Dutta [1,2,*] Avishek Maity [3,†] Anna Marsicano [4] J. Ross Stewart,[5] Matthias Opel [6] and Werner Paulus [4]

[1]*Institut für Kristallographie, RWTH Aachen Universität, 52066 Aachen, Germany*
[2]*Jülich Centre for Neutron Science at Heinz Maier-Leibnitz Zentrum, 85747 Garching, Germany*
[3]*Heinz Maier-Leibnitz Zentrum, Technische Universität München, 85747 Garching, Germany*
[4]*Institut Charles Gerhardt Montpellier, Université de Montpellier, 34095 Montpellier, France*
[5]*ISIS Neutron and Muon Source, Rutherford Appleton Laboratory, Didcot OX11 0QX, United Kingdom*
[6]*Walther-Meißner-Institut, Bayerische Akademie der Wissenschaften, 85748 Garching, Germany*

We report an inelastic neutron scattering study (INS) on the low-energy crystal electric field (CEF) excitations of Pr$_{2-x}$Sr$_x$NiO$_{4+\delta}$ single crystals at various temperatures. The observed low-E CEF level of the O-doped sample ($x = 0$, $\delta \approx 0.24$) at ~5.5 meV appears at significantly lower energy than that of the Sr-doped sample ($x = 0.5$, $\delta = 0.0$) at ~8.5 meV. Applying the point charge (PC) model calculation, this has been interpreted as an effect of the interstitial oxygen via lowering the local symmetry and modifying the CEF environment of the central rare earth Pr^{3+} ($^3H_4$) ions.

I. INTRODUCTION

Complex oxides in the family of strongly correlated electron systems involving both $4f^n$ lanthanide and $3d^n$ transition metal ions exhibit a rich variety of novel phenomena due to a combination of their electronic interactions of spin, orbital and charge degrees of freedom [1–4]. *214*-nickelates, cobaltates, and cuprates fall into these similar categories and their magnetism either Néel or stripe antiferromagnetic (AFM) differs depending on the corresponding spin states of the divalent transition metal (TM) ions Ni^{2+} ($S = 1$), Co^{2+} ($S = 3/2$), and Cu^{2+} ($S = 1/2$), respectively [5–8]. The underlying magnetism becomes more complicated by the presence of magnetic trivalent lanthanide (*Ln*) ions (*Ln* = Pr, Nd, Sm) in comparison to the nonmagnetic La^{3+} [9–11]. In some cases the polarizing effect, i.e.. the internal magnetic fields acting on the *Ln* sites induced by the ordered magnetic moment of the TM ions or vice versa, plays an active role determining the microscopic electronic and magnetic ground state [12–14]. Despite such polarization, *Ln*$^{3+}$ posses unique single-ion like character defined by the local CEF which splits the $4f^n$ electronic states into a series of energy levels determining the overall magnetic and physical properties of the system. The CEF potential contains crucial information on the local electronic structure and the ground state of the system.

Studies of the parent (Nd, Pr)$_2$NiO$_4$ show that the Kramers Nd^{3+} ions start to order antiferromagnetically below 10 K with magnetic moment ($3.2\mu_B$) at 1.5 K while the non-Kramers Pr^{3+} ions order partially or remain almost in paramagnetic singlet ground state even below 1.5 K [15,16].

There are differences as well in the CEF excitations with doping. In both, parent and doped (Sr = 0.4) Nd-nickelates, the lowest CEF excitation of Nd^{3+} has been observed almost at same energy (~8 meV) [17], while the lowest CEF excitation in the parent Pr$_2$NiO$_4$ has been reported at ~4.3 meV [18]. However, Pr^{3+} and Nd^{3+} ions differ from each other to a greater extent in terms of $4f^n$ splitting by the CEF and the polarizing effect by the ordered Ni^{2+} spin sublattice. Nonetheless, to our knowledge, so far there have been no further studies on the Sr/O-doped Pr-nickelates reporting on low energy CEF excitations. Therefore it is important to investigate the CEF excitations of Sr/O-doped Pr-nickelates to understand the cooperative interplay of electronic correlations of Pr^{3+} under different CEF potentials due to different types of doping.

In this paper, we present a detailed study of the CEF excitations of Pr$_{1.5}$Sr$_{0.5}$NiO$_4$ (PSNO) and Pr$_2$NiO$_{4.24\pm0.01}$ (PNO) single crystals, both of which lie at the higher doping sides of Pr$_2$NiO$_4$ with an electronically equivalent doping concentration ($n_h = x + 2\delta$), especially showing the effect of interstitial oxygen (O$_{int}$) on the Pr^{3+} CEF excitations in comparison with Sr doping by looking at low energy INS spectra. However, the Sr- and O-doped compounds do not align apparently in terms of the crystal field environment and the electronic states of the localized Pr^{3+} ion. We have used PC model simulation incorporating the local CEF environment in both compounds to explain the observed CEF excitation of Pr^{3+} and the models are verified against the directionally dependent magnetic susceptibility and magnetization curves. Interestingly, in the case of the PNO sample, incorporating excess O$_{int}$, nominally one per unit cell, lowers the local symmetry of those particular Pr atoms close to the O$_{int}$ resulting in different crystal field splitting compared to those Pr atoms without a nearby O$_{int}$. Our study indicates the importance of including the actual

---

*Corresponding author: rajesh.dutta@frm2.tum.de
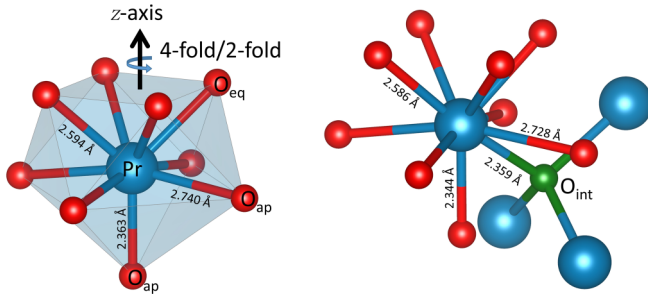†Corresponding author: avishek.maity@frm2.tum.de

FIG. 1. (Left) Capped-square antiprism CEF environment of Pr^{3+} ion with fourfold or twofold rotational z axis (black arrow) of the local point symmetry in case of $4/mmm$ or mmm, respectively. (Right) CEF environment with an extra O_{int} (green).

CEF environment in the PC modeling in order to describe the related single-ion properties.

II. METHODS

We have used the single crystals of PSNO and PNO taken for our previous studies [19–21] and the INS experiments are performed on the thermal triple-axis spectrometer (TAS) PUMA [22] at Heinz Maier-Leibnitz Zentrum, Germany and on the thermal neutron time-of-flight(TOF) chopper spectrometer MAPS [23] at the ISIS Neutron and Muon Source of the Rutherford Appleton Laboratory, UK. The details of the experimental methods are described in references [19–21]. Additional macroscopic magnetic measurements on both samples have been performed using a superconducting quantum interference device (SQUID) magnetometer under DC mode (MPMS XL7-Quantum Design Inc., San Diego, CA) at the Walther-Meißner-Institut, Germany.

III. RESULTS AND DISCUSSION

PSNO (mass = 5 g) crystallizes in tetragonal structure with space group $I4/mmm$ and lattice parameters $a = 3.78$ Å and $c = 12.54$ Å, where the onset of the Ni^{2+} spin-stripe ordering takes place below 130 K, whereas for PNO, it takes place almost at room temperature (RT) but start to become pronounced below ≈ 220 K. PNO (mass = 3.5 g) crystallizes in a monoclinic structure adopting space group $F112/m$ and lattice parameters $a = 5.39$ Å, $b = 5.45$ Å, $c = 12.44$ Å, and $\gamma = 90.03°$. The monoclinic symmetry implies an additional complexity related to twin domains as further outlined in the references [24,25]. This leads to a pseudomerohedrical overlay of satellite reflections related to the only small deviation from an orthorhombic symmetry ($Fmmm$) as the monoclinic angle is $90.03°$. However, the established long-range O ordering will certainly imply a well defined atomic positions even though of low point symmetry of Pr. Since the deviation from an orthorhombic symmetry is only minor, we have chosen the respective $Fmmm$ unit cell for theoretical PC modeling. This turned out to be still a good choice, although the real point symmetry is supposed to be lower.

Figure 1 shows only the Pr-polyhedra in both cases of doping. In the PSNO, Pr^{3+} ions have capped-square antiprism-type coordination by three sets of nonequal Pr–O

bonds and are kept at a long distance in the structure not being influenced by the ordered magnetic moments of the Ni^{2+} sublattice. However, in case of PNO with $Fmmm$ setting as there will be one O_{int} in the unit cell occupying any of the eight possible Wyckoff position $8f$ (1/4, 1/4, 1/4), we have to consider two sets of Pr polyhedra, one with a nearby O_{int} and other without the nearby O_{int}. Using these structural input we have carried out PC calculations using PYCRYSTALFIELD software [26] to simulate the experimental neutron spectrum and SQUID data.

In order to describe the experimental observation, we start with building the CEF Hamiltonian from Coulombic repulsion for the PC calculation treating the surrounding ligands (O) as point charges ($2e$) and the Hamiltonian can be written as

$$\mathcal{H}_{CEF} = \sum_{n,m} B_n^m O_n^m, \qquad (1)$$

where B_n^m are so-called CEF parameters and O_n^m are the Stevens operators with $-n \geqslant m \geqslant n$. In general for the rare earth (RE) ion, $4f$ electrons are more shielded from their ligands than $3d$ TM electrons, leaving the crystal field weak compared to the spin-orbit interaction. Thus J becomes a good quantum number in RE ions. For our calculation we stick to the J basis for Pr^{3+}. To have nonzero CEF parameters of the central ion and to eliminate the imaginary CEF operators one needs to find the y axis normal to the mirror plane and the z axis along the highest rotation axis. In the tetragonal case of PSNO the z axis lies along the fourfold rotation axis of the crystal structure (left in Fig. 1). Howeevr, in PNO, we have two different CEF environments: one without O_{int} where the z axis is along twofold rotation axis (similar to left in Fig. 1) and the other with O_{int} where the corresponding high-symmetry z axis is absent but the y axis perpendicular to the diagonal (110) mirror plane passing through O_{int}.

We start with the discussion of results from the PSNO sample followed by the comparison with the results from PNO sample. Two-dimensional (2D) energy-momentum (E-Q) maps and the corresponding one-dimensional (1D) line cuts of excitation spectra of PSNO are shown in Figs. 2(a), 2(b) and 2(c), 2(d), respectively. These line cuts were chosen in such a way that they do not include any elastic signal from the spin stripe ordering and nuclear Bragg peaks. Thus intensity at $E = 0$ meV is solely coming from incoherent scattering as there is no intensity expected from the calculation for the ground state CEF of Pr^{3+} at low-T. The low lying CEF excitations appears at ~ 8.85 meV with a broad full-width at half maxima (FWHM) ~ 5.5 meV where the instrumental resolution is only 2.8–3 meV. Pr^{3+} ion with $4f^2$ electron has quantum numbers $S = 1$ and $L = 5$ giving rise to an effective $J = 4$ by Hund's rule and under the CEF it splits the electronic states into two doublets and five singlets for d_{4h} symmetry. In this configuration, we have five nonzero B_n^m CEF parameters namely B_2^0, B_4^0, B_4^4, B_6^0, and B_6^4 which are given in the Table I considering effective oxygen charge to be $2e$. We found these B_n^m parameters are almost robust even if we consider the effective oxygen charge to be $1.7e$ (see the Table I). However, the second excited doublets predicted at 34.85 meV was difficult to identify because of the weak and broad intensity distribution of the spectra in this energy range
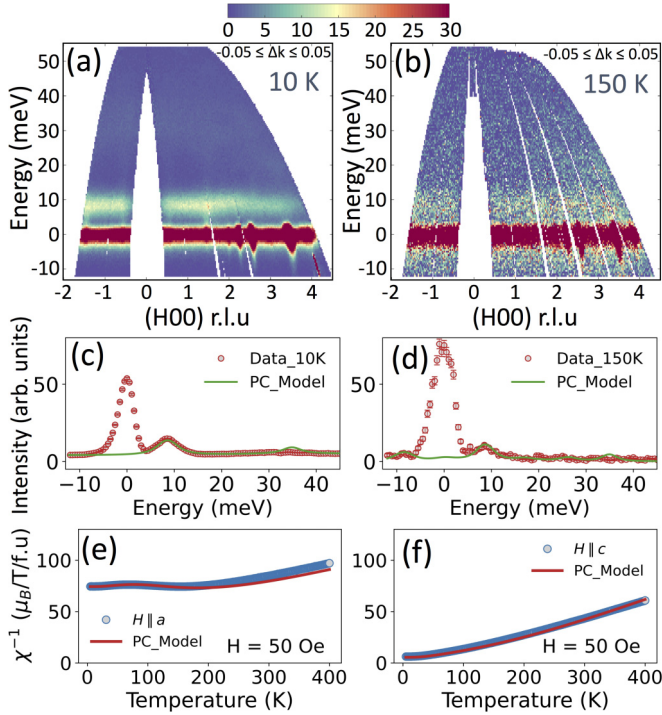
FIG. 2. The INS spectra of PSNO measured at MAPS spectrometer with incident neutron energy $E_i = 60$ meV at (a) 10 and (b) 150 K. Corresponding 1D line cuts at (100) with $0.95 \leqslant \Delta h \leqslant 1.05$ (r.l.u) are shown in (c) and (d) with vertical error bars, where the solid green lines represent the calculated CEF excitations from the PC model. Inverse magnetic susceptibility along the crystallographic (e) a and (f) c axes where the solid red lines are the calculated inverse susceptibility of Pr^{3+} using PC model.

of 25 to 40 meV [as visible in the color map in Fig. 2(a)], which includes contribution as well from magnons [20]. Rest of the eigenvalues show no intensity in the PC model calculation similar to the experimental data. As we have found only

TABLE I. Calculated CEF parameters from PC model with the effective charge $2e$/O except the third column.

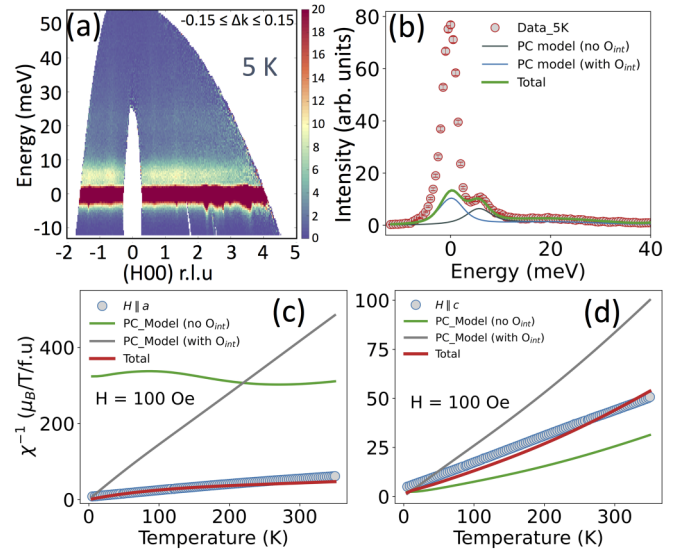| B_n^m (meV)	PSNO	PSNO ($1.7e$/O)	PNO (no O_{int})	PNO (with O_{int})
B_2^0	−1.0603	−0.9807	−1.4961	−0.8854
B_2^1				−8.2417
B_2^2			−0.1253	−0.0882
B_4^0	−0.0047	−0.0043	−0.0064	0.0003
B_4^1				0.0124
B_4^2			0.0021	0.0026
B_4^3				0.0978
B_4^4	0.0644	0.0595	−0.0578	−0.0361
B_6^0	9.204×10^{-5}	8.514×10^{-5}	0.0001	0.0001
B_6^1				−0.0004
B_6^2			1.974×10^{-5}	3.116×10^{-5}
B_6^3				−0.0004
B_6^4	0.0029	0.0027	−0.0027	−0.0038
B_6^5				−0.0023
B_6^6			8.157×10^{-5}	9.856×10^{-5}

FIG. 3. (a) The INS spectra of PNO measured at MAPS spectrometer with incident neutron energy $E_i = 60$ meV at 5 K and the corresponding 1D line cuts at (100) with $0.95 \leqslant \Delta h \leqslant 1.05$ (r.l.u) are shown in (b) with vertical error bars, where the solid lines represent the calculated CEF excitations from the point charge (PC) model with two sets of CEF environment. Inverse magnetic susceptibility along the crystallographic (c) a and (d) c axes where the solid lines are the calculated susceptibility using PC models.

one strong CEF excitations in the INS spectrum measured up to 54 meV and we have five CEF parameters, we avoid fitting the spectra, rather it has been simulated. To show that the intensity of the CEF excitation peak at 8.85 meV is coming from Pr^{3+} ions, we have compared the intensity fall with the calculated magnetic form factor of Pr^{3+}, see Fig. 4(a).

However, to have a confidence on the calculated CEF parameters, we have calculated the magnetic susceptibility with the predicted CEF parameters and we have found a fine agreement with the experiment shown in Figs. 2(e) and 2(f). For the magnetic susceptibility, it should be noted that the system contains two magnetic ions Pr^{3+} and Ni^{2+}. Susceptibility (χ_m) and the magnetization (M-H) curves of Pr^{3+} ion were calculated using an effective Hamiltonian $\mathcal{H}_{CEF} + \mu_B g_J \mathbf{B.J}$ under the applied external magnetic field B. Calculated χ_m^{-1} along the crystallographic c direction reproduces adequately the experimental observation down to 5 K, whereas along a axis a certain deviation occurs above 150 K, see Figs. 2(e) and 2(f). Such deviation comes from the Ni^{2+} paramagnetic contribution since the Ni^{2+} spin-stripe ordering does not get fully established at this temperature. Below 150 K more or less the features of χ_m^{-1} comes from the crystal field of Pr^{3+} ions and they do not order magnetically down to 10 K as verified in the excitation spectra and calculation due to its crystal-field induced singlet ground state.

Now, we switch to PNO sample where we have much more complicated situation regarding CEF environment. Figures 3(a) and 3(b) display the CEF excitations spectrum obtained at 5 K. The low energy CEF level is observed at ~6 meV but with less FWHM ~4 meV compared to PSNO sample. This might be due to the absence of Sr disorder in PNO sample. First, we considered the CEF environment of
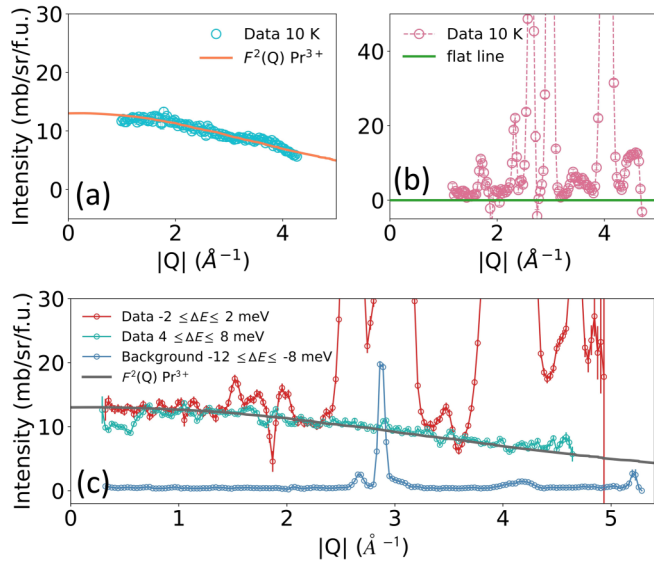
FIG. 4. (a) Integrated intensity of the INS spectrum of PSNO over the energy range $6 \leqslant \Delta E \leqslant 10$ meV in Fig. 2(a) where the orange solid line represents the calculated magnetic form factor of Pr^{3+} ion. (b) Integrated intensity of the INS spectrum of PSNO around the elastic scattering line over the energy range $-2 \leqslant \Delta E \leqslant 2$ meV where the flat green solid line is the eye guide to zero intensity. In both cases the intensity integration has been performed taking into account fixed $-0.3 \leqslant \Delta k \leqslant -0.2$ along $(h, -0.1, 0)$. Strong intense peaks in (b) are coming from Bragg scattering. (c) Integrated intensity of the INS spectrum of PNO over the energy range $-2 \leqslant \Delta E \leqslant 2$ meV (red), $4 \leqslant \Delta E \leqslant 8$ meV (cyan) and $-12 \leqslant \Delta E \leqslant 8$ meV (blue), where the grey solid line represents the calculated magnetic form factor of Pr^{3+} ion. The intensity integration has been performed taking into account fixed $-0.3 \leqslant \Delta k \leqslant -0.2$ along $(h, -0.1, 0)$.

Pr without O_{int}, i.e., with only nine oxygen atoms as ligands similar to Fig. 1 (left) but having twofold rotational axis along z in the orthorhombic d_{2h} symmetry where only 9 nonzero B_n^m parameters are allowed. Using this particular setting with the B_n^m parameters listed in Table I, it gives rise to a strong peak at ~ 6 meV but the calculated χ_m [green curves in Figs. 3(c) and 3(d)] using these B_n^m parameters does not reproduce the experimental χ_m^{-1} curves. To look for the reason behind such discrepancies between the calculated and experimentally observed data we have decided to include the O_{int} [Fig. 1 (right)] in the calculation to represent Pr-CEF environment in a better way. We have considered two sets of Pr-CEF. The first set contains 9/4 Pr atoms out of 8 Pr atoms of the PNO unit cell which will have the O_{int} in the CEF environment as the O_{int} will be shared by the nearby 4 Pr atoms independent of which Wyckoff postion is occupied by O_{int} and the second set contains rest 23/4 Pr atoms which will have no O_{int} in the CEF environment. This information is crucial as the relative intensity of the CEF excitation calculated per formula unit will depend on these two sets of Pr atoms which will be treated as an overall scale factor. However, we had to consider these two Pr-CEF sets in our calculations separately and afterwards we performed the weighted sum of calculated spectra according to the overall scale-factor as the CEF is after all a single-ion property. This avoids overestimating the CEF spectral intensity.
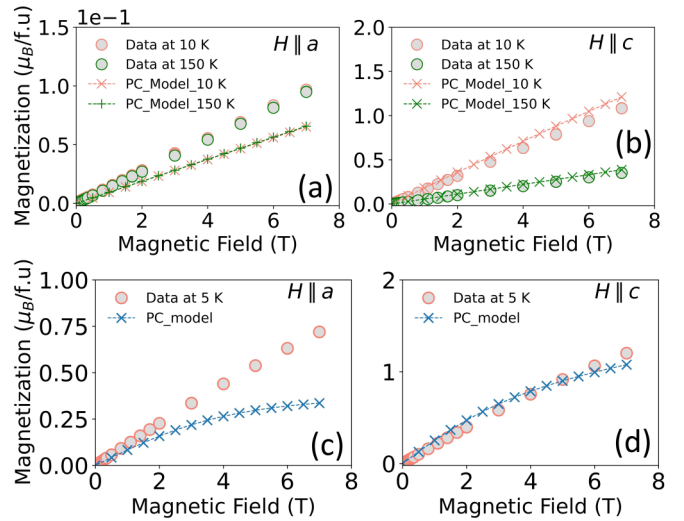

FIG. 5. Measured and simulated magnetization curves along the crystallographic a and c axes for the sample [(a) and (b)] PSNO and [(c) and (d)] PNO.

However, as it is easily noticeable in the Fig. 1 (right) that inclusion of O_{int} does not preserve the twofold rotation along z axis anymore even in the $F112/m$ setting rather reduces it to lower symmetry (c_1) which gives 15 nonzero B_n^m parameters out of 26 total parameters. Since the diagonal (110) mirror plane containing the O_{int} still exists, it eliminates the other total of 11 imaginary B_n^m parameters. With this setting calculated CEF excitations give rise to a peak at ~ 0.25 meV [blue curve in Fig. 3(b)]. It is difficult to identify this peak from our INS measurements as it is near the zero energy incoherent scattering. Nonetheless we have obtained a satisfactory agreement with the measured χ_m^{-1} using these two sets of Pr-CEF environment; with and without O_{int}, in Figs. 3(c) and 3(d). Red curves represent the combined signal after considering the overall scale factor from both Pr-CEF sets. In addition to the $|Q|$ dependency of the excitation peak intensity at ~ 6 meV, the integrated intensity around the elastic line follow the magnetic form factor of Pr^{3+} as presented in Fig. 4(c), indicating the possible existence of the lowest excited CEF peak at ~ 0.25 meV as calculated whereas Fig. 4(b) shows no such $|Q|$ dependency in PSNO sample indicating no such presence of CEF state close to zero.

Additionally, we have carried out the calculation of magnetization curves for the both PSNO and PNO samples which are shown in Figs. 5(a), 5(b) and 5(c), 5(d) respectively. Only Pr sublattice magnetization obtained from PC model are shown. In the PSNO sample magnetization curves show typical AFM signal up to 7 T, whereas in PNO sample there is a saturation like tendency at higher field. and this is more likely from Pr atoms. For both samples, calculated magnetizations along c axis follows nicely with the experimental data than that along a axis. This also indicates that in the ab plane Ni sublattice magnetizations needs to be included in order to have better agreement with the experimental data. However, magnetic susceptibility and magnetization curves are highly anisotropic indicating the c axis as an easy axis for Pr^{3+}. The single ion anisotropy of Pr atoms in terms of 3D
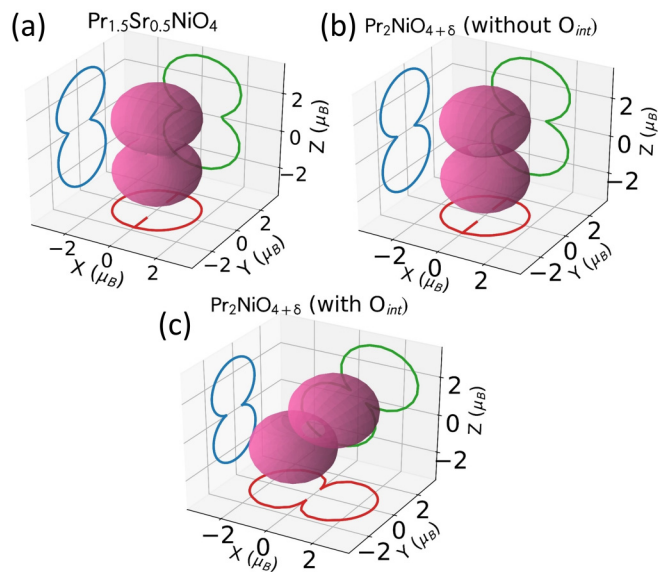
FIG. 6. 3D plots of saturation magnetization representing the Pr single ion anisotropies of PSNO and PNO, in various directions at 10 K computed from the CEF parameters using the field of 150 T. The colored traces indicate the outline of the 3D figure along the x, y, and z directions.

IV. CONCLUSION

In summary, crystal electric field excitations of Pr based *214*-nickelates are investigated by using INS and macroscopic magnetization measurements where the effect of an interstitial oxygen in the O-doped sample has been revealed through CEF excitations in comparison with the Sr-doped sample. Our point charge models adequately reproduces the strong low-E CEF excitation peak in the INS spectrum for both sample. In addition, the calculated magnetic susceptibility together with magnetization curve based on CEF parameters indicate the nature of ground and excited states of Pr atoms depending on CEF environments. Sr-disorder might accounts for the broadening of CEF excitations linewidth, in contrast ordered O_{int} may help narrowing the linewidth of the CEF excitation in case of O-doped sample. Additionally, from PC calculation O-doping reveals a low-lying excited state near the zero energy ground state which was necessary to interpret the characteristics of susceptibility data. In addition, the effect of O_{int} on the anisotropy magnetization surfaces is also revealed. Specially, this study highlights the importance of considering the both high and low symmetry Pr-CEF environments in the presence of O_{int}. Further investigations on the CEF contribution from Ni octahedra relatively at high energy ($> 100\,meV$) might benefit such study.

MAPS data are available at ISIS Neutron and Muon Source Data Journal in Ref. [27].

magnetization density distribution is calculated from the saturation magnetization using the CEF parameters listed in Table I for the PC calculation with $2e$/O. The anisotropy surfaces of magnetization for PSNO and PNO samples are displayed in the Fig. 6. Figure 6(a) clearly indicates that the anisotropy surefaces for the PSNO sample is pointing towards c axis. For PNO sample the anisotropy surfaces are treated separately (with and without O_{int}). Without O_{int} the anisotropy surface in Fig. 6(b) is similar to the PSNO but including O_{int}, Fig. 6(c) clearly shows the significant effect of the O_{int} on changing the anisotropy surface.

[1] E. S. Clementyev, P. A. Alekseev, V. V. Efimov, I. O. Troyanchuk, A. S. Ivanov, V. N. Lazukov, and V. V. Sikolenko, Crystal electric field effects in $Pr_{0.5}Sr_{0.5}CoO_3$, J. Synch. Investig. **6**, 553 (2012).

[2] A. Bhattacharyya, D. T. Adroja, A. M. Strydom, A. D. Hillier, J. W. Taylor, A. Thamizhavel, S. K. Dhar, W. A. Kockelmann, and B. D. Rainford, μSR and inelastic neutron scattering investigations of the noncentrosymmetric antiferromagnet $CeNiC_2$, Phys. Rev. B **90**, 054405 (2014).

[3] A. J. Princep, D. Prabhakaran, A. T. Boothroyd, and D. T. Adroja, Crystal-field states of Pr^{3+} in the candidate quantum spin ice $Pr_2Sn_2O_7$, Phys. Rev. B **88**, 104421 (2013).

[4] Z. Jirák, J. Hejtmánek, K. Knížek, M. Maryško, P. Novák, E. Šantavá, T. Naito, and H. Fujishiro, Ground-state properties of the mixed-valence cobaltites $Nd_{0.7}Sr_{0.3}CoO_3$, $Nd_{0.7}Ca_{0.3}CoO_3$ and $Pr_{0.7}Ca_{0.3}CoO_3$, J. Phys.: Condens. Matter **25**, 216006 (2013).

[5] P. G. Freeman, A. T. Boothroyd, D. Prabhakaran, and J. Lorenzana, Magnetization of $La_{2-x}Sr_xNiO_{4+\delta}$ ($0 \leqslant x \leqslant 0.5$): Spin-glass and memory effects, Phys. Rev. B **73**, 014434 (2006).

[6] L. M. Helme, A. T. Boothroyd, R. Coldea, D. Prabhakaran, C. D. Frost, D. A. Keen, L. P. Regnault, P. G. Freeman, M. Enderle, and J. Kulda, Magnetic order and dynamics of the charge-ordered antiferromagnet $La_{1.5}Sr_{0.5}CoO_4$, Phys. Rev. B **80**, 134414 (2009).

[7] J. M. Tranquada, Topological doping and superconductivity in cuprates: An experimental perspective, Symmetry **13**, 2365 (2021).

[8] J. M. Tranquada, Spins, stripes, and superconductivity in hole-doped cuprates, AIP Conf. Proc. **1550**, 114 (2013).

[9] M. F. Hundley, J. D. Thompson, S.-W. Cheong, Z. Fisk, and S. B. Oseroff, Specific heat and anisotropic magnetic suscepti-

bility of Pr_2CuO_4, Nd_2CuO_4 and Sn_2CuO_4 crystals, Physica C: Superconductivity **158**, 102 (1989).

[10] A. T. Boothroyd, A. Longmore, M. Castro, R. Burriel, and R. S. Eccleston, The magnetic states of R^{3+} in R_2NiO_4 (R = Pr, Nd), J. Phys.: Condens. Matter **9**, 2275 (1997).

[11] R. Sachidanandam, T. Yildirim, A. B. Harris, A. Aharony, and O. Entin-Wohlman, Single-ion anisotropy, crystal-field effects, spin reorientation transitions, and spin waves in R_2CuO_4 (R = Nd, Pr, and Sm), Phys. Rev. B **56**, 260 (1997).

[12] M. Földeáki, H. Ledbetter, and Y. Hidaka, Magnetic susceptibility of Pr_2CuO_4 monocrystals and polycrystals, J. Appl. Phys. **70**, 5736 (1991).

[13] X. Batlle, X. Obradors, and B. Martinez, Magnetic interactions, weak ferromagnetism, and field-induced transitions in Nd_2NiO_4, Phys. Rev. B **45**, 2830 (1992).

[14] M. T. Fernández-Díaz, J. L. Martínez, J. Rodríguez-Carvajal, J. Beille, B. Martínez, X. Obradors, and P. Odier, Metamagnetism in single-crystal Pr_2NiO_4, Phys. Rev. B **47**, 5834 (1993).

[15] M. T. Fernández-Díaz, J. Rodríguez-Carvajal, J. L. Martínez, G. Fillion, F. Fernández, and R. Saez-Puche, Structural and magnetic phase transitions in Pr_2NiO_4, Z. Phys. B **82**, 275 (1991).

[16] J. Rodríguez-Carvajal, M. T. Fernández-Díaz, J. L. Martínez, F. Fernández, and R. Saez-Puche, Structural phase transitions and three-dimensional magnetic ordering in the Nd_2NiO_4 oxide, Europhys. Lett. **11**, 261 (1990).

[17] A. T. Boothroyd, S. M. Doyle, M. P. Sridhar Kumar, D. McK. Paul, and R. Osborn, Crystal fields in $Nd_{2-x}Sr_xNiO_{4+y}$, J. Less-Common Met. **164-165**, 915 (1990).

[18] M. Castro, R. Burriel, J. Pérez, A. T. Boothroyd, A. Longmore, and R. Eccleston, Crystal-field energy levels on Pr_2NiO_4 by inelastic neutron scattering and heat-capacity measurements, Phys. B: Condens. Matter **234-236**, 728 (1997), proceedings of the First European Conference on Neutron Scattering.

[19] A. Maity, R. Dutta, and W. Paulus, Stripe discommensuration and spin dynamics of half-doped $Pr_{3/2}Sr_{1/2}NiO_4$, Phys. Rev. Lett. **124**, 147202 (2020).

[20] R. Dutta, A. Maity, A. Marsicano, J. R. Stewart, M. Opel, and W. Paulus, Direct evidence for anisotropic three-dimensional magnetic excitations in a hole-doped antiferromagnet, Phys. Rev. B **102**, 165130 (2020).

[21] A. Maity, R. Dutta, A. Marsicano, A. Piovano, J. R. Stewart, and W. Paulus, Magnetic excitations in long-range stripe-ordered $Pr_2NiO_{4+\delta}$, Phys. Rev. B **103**, L100401 (2021).

[22] O. Sobolev and T. P. Jitae, Puma: Thermal three axes spectrometer, J. Large-Scale Research Facilities **1** (2015).

[23] R. A. Ewings, J. R. Stewart, T. G. Perring, R. I. Bewley, M. D. Le, D. Raspino, D. E. Pooley, G. Škoro, S. P. Waller, D. Zacek, C. A. Smith, and R. C. Riehl-Shaw, Upgrade to the maps neutron time-of-flightchopper spectrometer, Rev. Sci. Instrum. **90**, 035110 (2019).

[24] R. Dutta, A. Maity, A. Marsicano, M. Ceretti, D. Chernyshov, A. Bosak, A. Villesuzanne, G. Roth, G. Perversi, and W. Paulus, Long-range oxygen ordering linked to topotactic oxygen release in $Pr_2NiO_{4+\delta}$ fuel cell cathode material, J. Mater. Chem. A **8**, 13987 (2020).

[25] A. Maity, R. Dutta, O. Sendtskyi, M. Ceretti, A. Lebranchu, D. Chernyshov, A. Bosak, and W. Paulus, Exploring fast room temperature oxygen diffusion in $Pr_2NiO_{4+\delta}$ stand-alone single-crystalline electrodes, Chem. Mater. **34**, 414 (2022).

[26] A. Scheie, *PyCrystalField*: software for calculation, analysis and fitting of crystal electric field Hamiltonians, J. Appl. Crystallogr. **54**, 356 (2021).

[27] R. Dutta *et al.*, Role of interstitial oxygen ordering on the spin excitation of $Pr_{2-x}Sr_xNiO_{4+\delta}$, STFC ISIS Neutron and Muon Source, https://doi.org/10.5286/ISIS.E.RB1920233-1 (2019).